Transactions of the Materials Research Society of Japan 32[2] 509-512 (2007)

In-flight Melting of Granulated Powders in Thermal Plasmas for Glass Production

Yaochun Yao, Md. M. Hossain, Yasuko Oyamatsu, Takayuki Watanabe, Fuji Funabiki* and Tetsuji Yano*

Dept. Environmental Chemistry and Engineering, Tokyo Institute of Technology, 4259 Nagatsuta, Yokohama 226-8502, Japan
Fax: 81-045-924-5416, e-mail: watanabe@chemenv.titech.ac.jp
* Dept. Chemistry and Materials Science, Tokyo Institute of Technology, S7-4, 2-12-1 O-okayama, Tokyo 152-8550, Japan

The innovative in-flight glass melting technology with thermal plasmas was developed for the purpose of energy conservation and environmental protection for glass production. Modeling and experiments of induction thermal plasmas have been performed to investigate the melting behavior of granulated powders injected into thermal plasmas. The thermofluid fields were obtained by solving two-dimensional modeling for argon plasmas under atmospheric pressure. Results show the strong influence of carrier gas flow rate on the melting behavior. With flow rate increasing, the particle size and temperature of glass transition and softening decrease, whereas the amount of unreacted SiO_2 increases because of lower plasma temperature and shorter residence time. The experimental results are consistent with the model, which gives valuable practical guidelines in optimizing the process parameters and controlling the product characteristics.
Keywords: Induction thermal plasmas; Glass production; In-flight melting; Plasma heat transfer

1. INTRODUCTION

Thermal plasmas have received many attention due to its high chemical reactivity, easy and rapid generation of high temperature, high enthalpy to enhance the reaction kinetic, large volume with low velocity, oxidation and reduction atmosphere in accordance with required chemical reaction as well as rapid quenching capability [1]. The thermal plasmas have been widely applied to many fields because of these unique advantages, such as synthesis of nanoparticles, chemical vapor deposition and plasma spraying. Recently, an attractive application is treatment of harmful waste materials and recovery of useful materials from wastes [2].

The glass industry has been using the traditional melting technology since 100 years ago. The typical system used for melting glass is refractory-lined melting furnace, fired by air or oxygen and natural gas or oil as fuel. Many improvements have been made in furnace life and energy efficiency, however, the fundamental technology has not been changed. Larger consumption of fossil fuel, longer melting time and higher emission are still the challenges confronting glass industries [3]. The glass demand in world is gradually increasing with the rapid development of architecture and automobile industries, so it is a crucial problem to increase the productivity, reduce the energy usage and lessen the environmental impact. The application of thermal plasmas into glass melting is one of the most promising technologies in contemporary glass production.

In this study, an innovative in-flight glass melting technology with thermal plasmas is developed to solve the above-mentioned shortcomings. The melted powders and glass were prepared by the radio-frequency (RF) induction thermal plasmas. The melting behavior of granulated powders injected with different carrier gas flow rates is characterized with XRD, SEM, TG-DTA and EPMA analysis. Finally, the experimental results are explained using the numerical analysis simulated with the two-dimensional model for argon plasmas under atmospheric pressure.

2. EXPERIMENTAL

2.1 Experimental procedures

Fig.1 presents a schematic illustration of experimental setup for in-flight melting of granulated powders. The experimental setup consists of a plasma torch, a reaction chamber and a power supply. The plasma torch consists of a water-cooled quartz tube and a working induction coil. The reaction chamber was set below the torch. The water-cooled substrate for collecting quenched powder or the refractory brick for collecting glass was placed in the

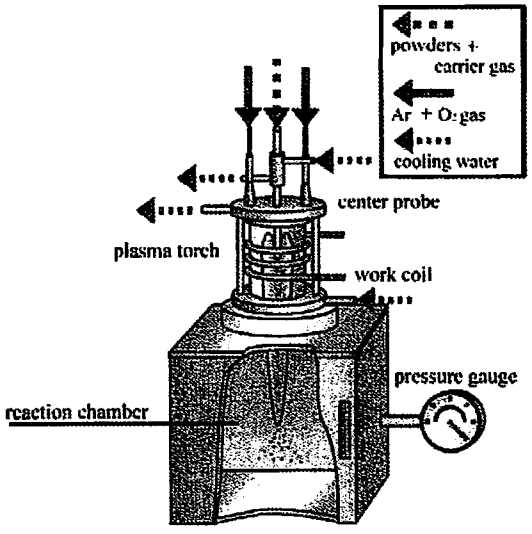

Fig.1. Schematic of experimental apparatus (RF plasma).

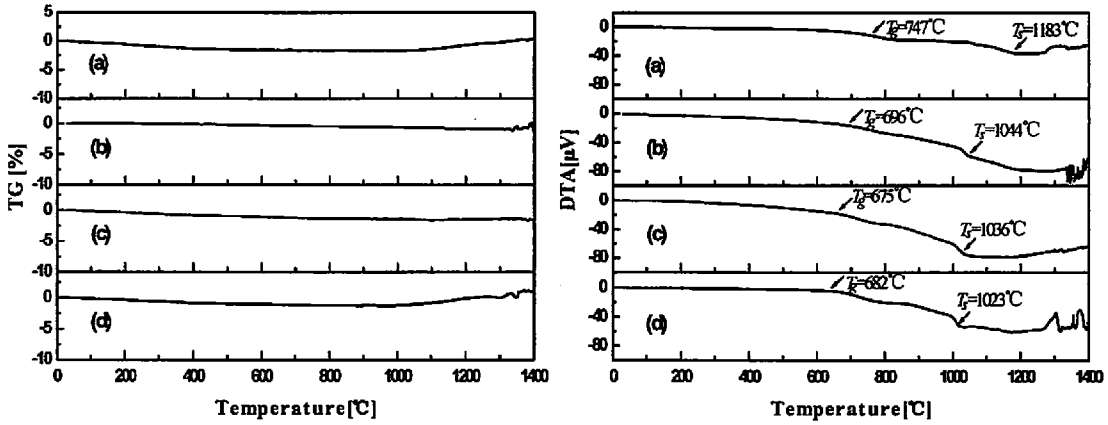

Fig.2. TG-DTA curves of quenched powders at different flow rates of carrier gas: (a) 3 l/min; (b) 4 l/min; (c) 5 l/min; (d) 6 l/min.

chamber. Typical operating conditions were as follows. Plate power: 20 kW; total pressure: 101.3 kPa; argon plasma gas: 2.0 l/min; sheath gas: 22 l/min (Ar) + 2 l/min (O_2); feed rate: 5 g/min (for quenched powders) and 10 g/min (for glass).

The granulated powders of raw material were prepared by the spray-drying method from the reagents of Na_2CO_3, $CaCO_3$ and SiO_2 for the soda-lime-silica glass. The raw material with about 58 μm in average diameter was injected into the thermal plasmas by a powder feeder. The prepared powders were quenched on a water-cooled substrate (T<30°C) at 340 mm from nozzle to substrate and the glass was collected on the refractory brick (T>1000°C) at the distance of 190 mm.

The thermogravimetric-differential thermal analyzer (TG-DTA) for thermal analysis was performed with thermogravimetry on TG8120 (Rigaku), the measured temperature in the range of 20~1400°C, at the rate of 10°C/min. The micrograph and size distribution of the particles was carried out by scanning electron microscope (SEM) on JSM5310 (JEOL). The structures of the prepared powders were determined by X-ray diffractometry (XRD). XRD was carried out on Miniflex (Rigaku) with Cu K_α radiation at 30 kV and 15 mA. The data were collected in the 2θ range 3-90° with a step size of 0.02° and a scan speed of 4°/min. The composition of glass was analyzed by electron probe microanalysis (EPMA) on JXA-8200 (JEOL).

2.2 Experimental results and discussion

2.2.1 Effects of carrier gas on quenched powders

The TG-DTA curves of quenched powders melted by RF plasma are shown in Fig.2. The TG curves show no obvious weight loss of the prepared samples in the temperature range of TG. It indicates the carbonates (Na_2CO_3 and $CaCO_3$) in raw material were almost 100% decomposed during in-flight melting by RF plasma. The DTA curves show that there are two small endothermic peaks corresponding to the temperature of glass transition (T_g) and softening (T_s). It could be seen that T_g and T_s decrease with the flow rate increasing, which reveals the flow rate of carrier gas has an influence on the composition of powders.

The XRD patterns of quenched powders at different flow rates of carrier gas are shown in Fig.3. There are not

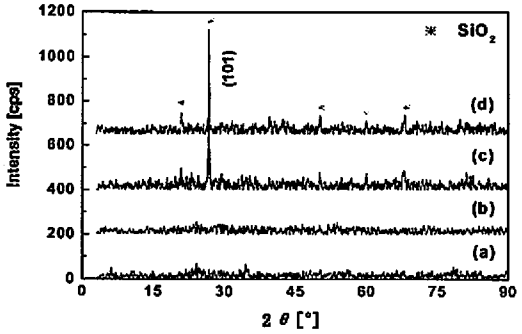

Fig.3. XRD patterns of quenched powders at different flow rates of carrier gas: (a) 3 l/min; (b) 4 l/min; (c) 5 l/min; (d) 6 l/min.

diffractive peaks in sample (a) and sample (b), which indicates that these powders are of amorphous structure with the glass characteristics, that is, they are not crystal substance. The difference of (101) peak intensity among samples reveals the different amount of SiO_2 crystal. The internal standard method with XRD is used to analyze reaction fractions quantitatively, ZnO as the internal standard. The reaction fractions are 99.7%, 99.4%, 97.7% and 94.8% in an increasing order of carrier gas. It is considered that larger carrier gas flow rate leads to lower plasma temperature and faster plasma velocity, so the decrease of reaction fraction of SiO_2 is caused by lower particle temperature and shorter residence time.

The morphology and particle size distribution of prepared powders at different flow rates of carrier gas are presented in Fig.4. The quenched particles have spherical shape, smooth surface and compact body. The peak of size distribution becomes narrower and higher, which indicates that larger flow rate of carrier gas is helpful to yield a uniform size of particles. In addition, the mean diameter of quenched powders reduces to almost one third of that of raw material and reduces as the carrier gas flow rate increases.

2.2.2 Effects of carrier gas on glass

To compare the difference in composition variation with powders, the glass samples with different flow rates of carrier gas were also synthesized. The photograph of one of glass samples is presented in Fig.5.

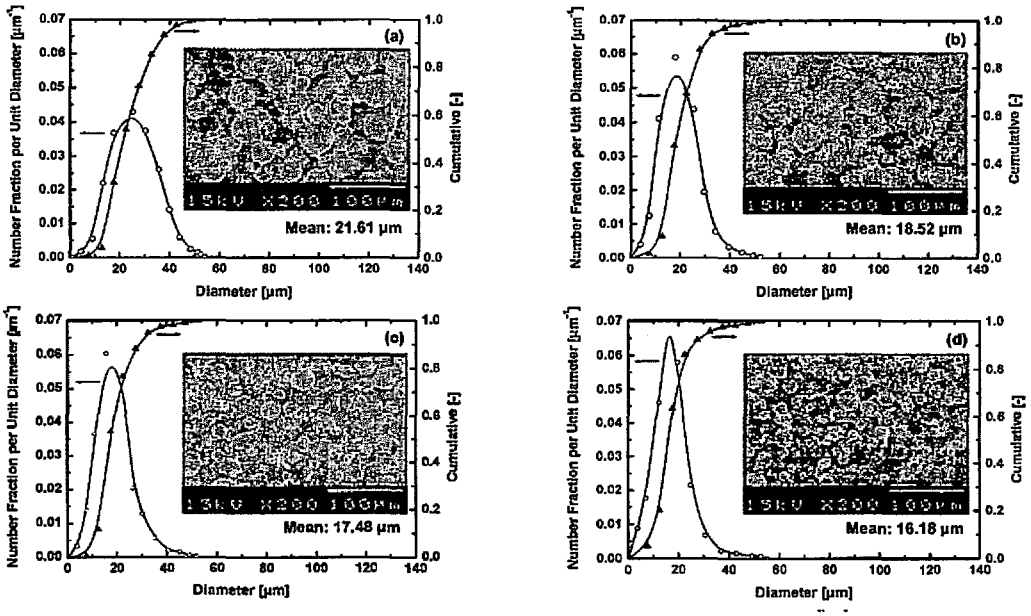

Fig.4. Particle size distribution and morphology of quenched powders at different flow rates of carrier gas: (a) 3 l/min; (b) 4 l/min; (c) 5 l/min; (d) 6 l/min.

Fig.5. Photograph of glass sample at the flow rate of 6 l/min and feed rate of 10 g/min.

As shown in picture, the glass is clear and transparent, indicating the vitrification of raw material completed during flight time. The average content of composition of glass and powders are analyzed, results shown in Fig.6. With the carrier gas flow rate increasing, the Na_2O content increases, the SiO_2 content decreases and the CaO content keeps almost same. The higher Na_2O and lower SiO_2 can be attributed to lower plasma temperature and shorter residence time caused by larger flow rate of carrier gas. Compared the variation of composition in powders and glass, the effect of carrier gas flow rate on glass is weaker than that on quenched powders because shorter collecting distance results in shorter residence time. The increase of Na_2O content in glass samples explains well the decrease of T_g and T_x in quenched powders. The function of Na_2O added in the soda-lime glass is to reduce the viscosity and melting temperature of glass by releasing the dissociative O and enhancing the ratio of O/Si in the process of melting. In addition, compared with the traditional air-fuel firing, the gas emission produced by thermal plasmas melting is less due to no use of fossil fuel.

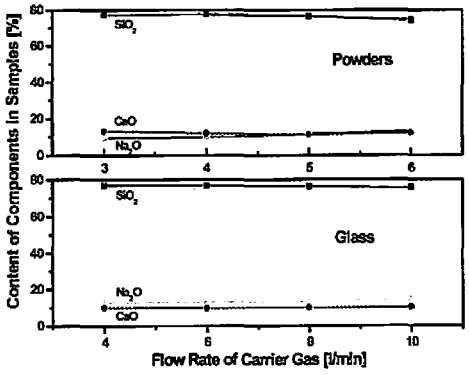

Fig.6. Variation of compositions of glass and powders as a function of carrier gas flow rate.

3. NUMERICAL ANALYSIS

The numerical model is based on Atsuchi et al. [4] and Mostaghimi et al. [5]. The conservation equations of mass, momentum, and energy along with the vector potential form of Maxwell's equations are solved simultaneously.

3.1 Thermodynamic and transport properties

The thermodynamic and transport properties of argon gas required for simulation include viscosity, specific at constant pressure, electrical and thermal conductivity, mass density and radiative loss coefficient. The transport properties, which are functions of temperature, were calculated under local thermodynamic equilibrium (LTE) conditions using Chapman-Enskog first approximation to the Boltzmann equation [6].

3.2 Assumptions and boundary conditions

The calculations are based on the following assumptions to solve the governing equation[4]: (a) steady-state laminar flow; (b) axial symmetry; (c) optically thin; (d) negligible viscous dissipation in energy equation; (e) negligible displacement current in comparison with the conductive current; (f) negligible flow-induced electric field; (g) same temperature of heavy particles and electrons.

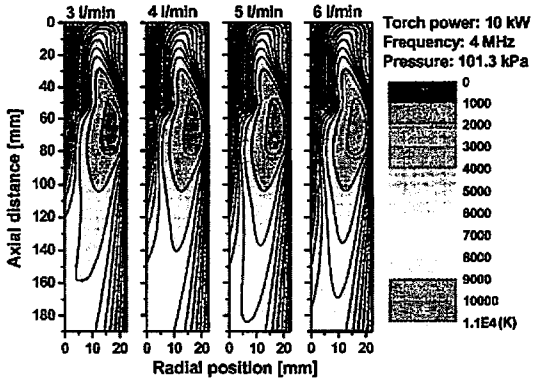

Fig.7. Isotherms of argon plasma at different flow rates of carrier gas at 4 MHz and 20 kW.

The boundary conditions along the centerline were set to insure the axial symmetry. At the wall of the plasma torch, no slip conditions are maintained for the velocity, and the concentrations have zero gradient. The temperature at the inside wall of the plasma torch was calculated assuming the outside wall was maintained at 300 K by water cooling. The injection tube was assumed to be at 300K. The outflow boundary conditions at the torch were assumed that gradient of the variables are zero.

3.3 Calculation procedure

The governing conservation equations were solved using the semi-implicit method for pressure linked equation revised (SIMPLER) algorithm [7]. The governing equations and the electric field intensity equation with the associated boundary conditions were discretized into finite difference form using the control volume technique. Non-uniform grid points 42 by 87 were used for radial and axial directions, respectively. Grids are made close to the center and the coil region.

3.4 Calculation results and discussion

The computations were performed for argon plasma operated under atmospheric pressure. The calculated temperature fields are shown in Fig.7. As the flow rate increases, the high-temperature region over 7000K in the torch shrinks and shifts far from the centerline.

The axial distribution of temperature and axial velocity at the center of quartz tube are presented in Fig.8. The temperature decreases with an increase of flow rate in Fig.8 (a). The Fig.8 (b) reveals that the maximum velocity of plasma is attained at the middle of the axial distance. The velocity of plasma is enhanced due to the larger momentum of carrier gas flow. These demonstrate that larger flow rate of carrier gas will lead to lower plasma temperature and faster plasma velocity. The lower temperature and faster velocity will result in lower volatilization of Na_2O and higher unreacted ratio of SiO_2, which are in agreement with the experiments results.

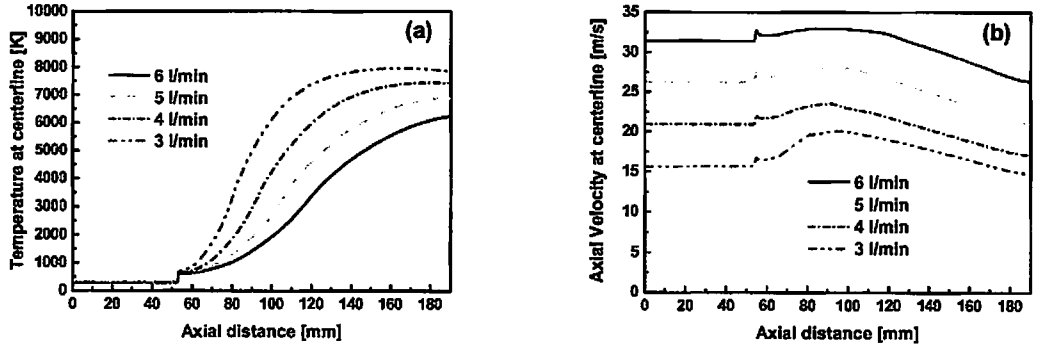

Fig.8. Axial distribution of temperature (a) and axial velocity (b) at the center of quartz tube.

4. CONCLUSION

The innovative in-flight glass melting technology with thermal plasmas was developed to save energy and protect environment.

Results show that the granulated powders (<100 μm) can be melted in microseconds by RF plasmas. The flow rate of carrier gas has a strong influence on the plasma temperature and velocity. Larger flow rate of carrier gas leads to lower softening temperature, lower reaction fraction of SiO_2 and higher Na_2O content, which are consistent with the results simulated by using the two-dimensional model.

The vitrification of raw material is almost 100% in the process of in-flight melting. The transparent glass was successfully synthesized with higher vitrification ratio under shorter time, whose composition is close to the common soda-lime glass.

Acknowledgements

The financial support provided by Strategic Development of Energy Conservation Technology Project of NEDO (New Energy and Industry Technology Development Organization) is gratefully acknowledged.

References

[1] T. Watanabe and N. Sugimoto, *Thin Solid Films*, **457**, 201-208 (2004).
[2] M. Sakano, M. Tanaka, T. Watanabe, *Thin Solid Films*, **386**, 189-194 (2001).
[3] R. Gonterman and M. Weinstein, *American Ceramic Society Bulletin*, **83**, 21-23 (2004).
[4] N. Atsuchi, M. Shigeta and T. Watanabe, *Int. Journal of Heat and Mass Transfer*, **49**, 1073-1082 (2006).
[5] J. Mostaghimi, K. C. Paul and T. Sakuta, *Journal of Applied Physics*, **83**, 1989-1908 (1998).
[6] D. Bruno, C. Catalfamo and A. Laricchiuta, *Physics of Plasmas*, **13**, 072307 (2006).
[7] S. V. Patanker, *"Numerical Heat Transfer and Fluid Flow"*, Ed. by M. A. Phillips and E. M. Millmon, McGraw-Hill, New York (1980) pp. 113-135.

(Received December 23, 2006;Accepted March 15, 2007)